A Short Analysis of the Effects of System Thermal Noise on Angle-of-Arrival Enhanced Range Profiles

by
Brett Borden
Research & Technology Division

FEBRUARY 1996

**NAVAL AIR WARFARE CENTER WEAPONS DIVISION
CHINA LAKE, CA 93555-6001**

Approved for public release; distribution is unlimited.

19960326 064

Naval Air Warfare Center Weapons Division

FOREWORD

The research described in this report was performed during fiscal year 1995 as part of an effort to improve radar classification and identification capabilities for noncooperative airborne targets. This problem continues to be a primary goal of radar research programs and considerable effort has been expended within the last few decades in attempts to solve it. The accuracy of these methods depends on available radar resolution and so, indirectly, depends on bandwidth.

A novel technique for radar-based noncooperative target recognition has been created and verified using synthesized data. The current work has concentrated on establishing performance criteria against the effects of system thermal noise errors.

This effort was supported by Office of Naval Research, Code 313.

This report was reviewed for technical accuracy by Carey Schwartz.

Approved by
R. L. Derr, *Head*
Research & Technology Division
February 1996

Released for publication by
S. HAALAND
Director for Research and Engineering

Under authority of
D. B. McKinney
RAdm., U.S. Navy
Commander

REPORT DOCUMENTATION PAGE

Form Approved
OMB No. 0704-0188

1. AGENCY USE ONLY *(Leave blank)*	2. REPORT DATE	3. REPORT TYPE AND DATES COVERED
	February 1996	Interim January—September 1995

4. TITLE AND SUBTITLE

A Short Analysis of the Effects of System Thermal Noise on Angle-of-Arrival Enhanced Range Profiles

5. FUNDING NUMBERS

N00014-94-WX-30309

6. AUTHOR(S)

Brett Borden

7. PERFORMING ORGANIZATION NAME(S) AND ADDRESS(ES)

Naval Air Warfare Center Weapons Division
China Lake, CA 93555-6001

8. PERFORMING ORGANIZATION REPORT NUMBER

NAWCWPNS TP 8283

9. SPONSORING/MONITORING AGENCY NAME(S) AND ADDRESS(ES)

W. J. Miceli
Office of Naval Research
Code 313
800 North Quincy Street
Arlington, VA 22217-5660

10. SPONSORING/MONITORING AGENCY REPORT NUMBER

11. SUPPLEMENTARY NOTES

12A. DISTRIBUTION/AVAILABILITY STATEMENT

A Statement; public release; distribution unlimited.

12B. DISTRIBUTION CODE

13. ABSTRACT *(Maximum 200 words)*

(U) This report documents an effort to modify the effects of thermal noise error on a novel automatic target recognition technique applicable to airborne radar targets. The method uses the information about the target's cross-range structure that is statistically encoded in the radar tracking data and is potentially applicable to many existing radar missile systems.

14. SUBJECT TERMS

Target Recognition
Radar
Range Profile

15. NUMBER OF PAGES

13

16. PRICE CODE

17. SECURITY CLASSIFICATION OF REPORT	18. SECURITY CLASSIFICATION OF THIS PAGE	19. SECURITY CLASSIFICATION OF ABSTRACT	20. LIMITATION OF ABSTRACT
UNCLASSIFIED	UNCLASSIFIED	UNCLASSIFIED	UL

INTRODUCTION

Previously, a novel technique for extending the information available from range profiles of airborne radar targets has been developed and applied to the problem of automatic target recognition (References 1 and 2). Since so much of the target shape information is tied up in the cross-range part of the radar "image", the principal difficulty with down-range profile techniques has been the limited target information available for classification purposes. Usual (e.g., Inverse Synthetic Aperture Radar, or ISAR) schemes are often unable to obtain this cross-range information because accurate association of aperture (induced by target motion) with data (collected over time) is very difficult (see Reference 1). The alternate method that has been proposed uses data collected over an *unknown* aperture and does not require range-induced-phase adjustments across the set of measurements. In addition, the technique is not affected by aspect-induced scintillation. This statistical approach makes use of the fact that the spatial derivatives of the scattered field phase are independent of range-induced phase shifts and depend upon the cross-range extent of the target.

The present discussion reports on efforts we have made to examine the sensitivity of this "enhanced range profile" technique to thermal noise in radar tracking systems. We begin by reviewing the algorithm itself and by developing the relevant ideas. Then we analyze the noise process, estimate its effects, and show some example results.

BACKGROUND AND MOTIVATION

Angle-Of-Arrival (AOA) measurements have been used for target tracking purposes for many years. So-called "phase monopulse" systems estimate the phase-gradient of the scattered field by differencing the outputs of closely spaced antennas. The direction of this gradient will lie normal to surfaces of constant phase (phase fronts). When the target is a point scatterer, the phase fronts will be spherical and centered on the target, and their normal directions will indicate target bearing. Of course, targets are not individual point scatterers and the phase-gradient will not always point to the target. The difference between actual target bearing and that estimated by the phase-gradient is known as target "glint error" and depends upon overall target structure.

A short radar pulse incident on a target can be used to isolate separate down-range target elements (see Figure 1). This is the idea behind "range profiles" which are maps of scatterer reflectivity as a function of range. By combining short pulses with high-resolution tracking, target *subcomponent bearing directions* can sometimes be determined as a function of range as well (Reference 3). This can occur, for example, if there is only one target scattering element per down-range "slice." Unfortunately, targets are usually sufficiently complex that each slice will generally contain more than one point scatterer and interference effects (scintillation) will preclude accurate single-measurement bearing estimates. Statistical estimates based on multiple measurements are required instead.

When a set of AOA measurements are collected from a maneuvering target over a short time interval, the effective (synthetic) aperture may be assumed to be small. If the target's aspect cannot
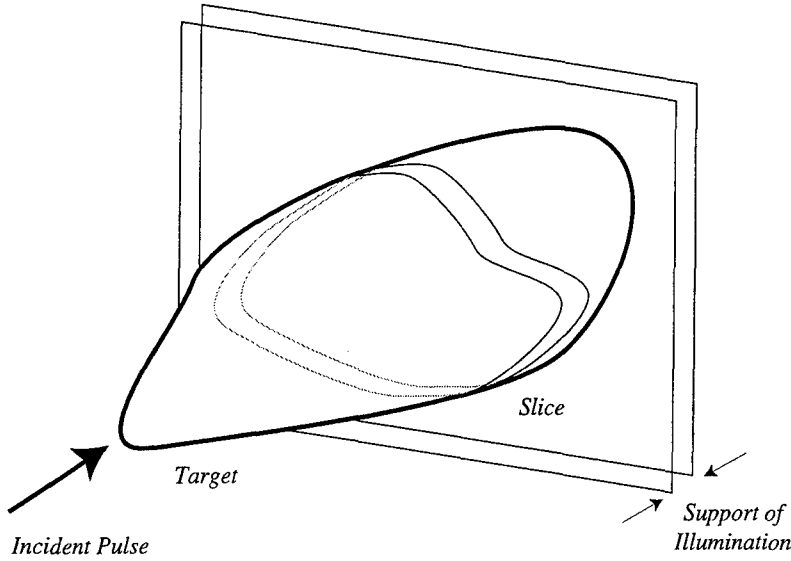
FIGURE 1. The Radar Pulse. A narrow radar pulse incident upon a target
will illuminate only a range "slice" at any particular instant.

be accurately determined over the set of AOA measurements, then the glint error can be considered
to be a function of random aspect angles. Let ϕ denote the phase of the scattered field E so that
$E = |E| \exp(i\phi)$. Then the cross-range component of the phase gradient along a direction θ (see
Figure 2) is given by

$$g(\theta) \equiv (\hat{\imath}\cos\theta + \hat{\jmath}\sin\theta) \cdot \nabla\phi. \qquad (1\ )$$

This will be the ideal measurement made by two closely spaced antennas lying along the θ direction.
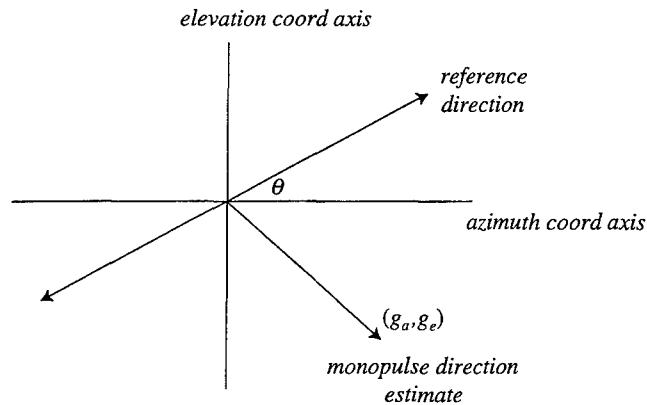

FIGURE 2. The Radar Coordinates. Here, $g_a \equiv g(\theta=0)$ and $g_e \equiv g(\theta=\pi/2)$
denote the components of the measured target bearing in the azimuth and
elevation directions, respectively.

2

Let $\rho(x,y)$ denote the local scattering reflectivity of the target at position (x,y) defined with respect to the origin (x_{ave}, y_{ave}) (see Figure 3). When the target is complex (the number of scattering centers is large), the central limit theorem implies that E is normally distributed and, at high radar frequencies, has zero mean. The statistics of g follow from a straightforward, although somewhat lengthy, calculation (Reference 2). The probability density of g is given by

$$f_g\left(g;\theta\right) = \frac{\kappa^2}{2\left(\kappa^2 + g^2\right)^{3/2}}, \tag{2}$$

where

$$\kappa^2\left(\theta\right) \equiv \int_{\mathbb{R}^2} \left|\rho\left(x',y'\right)\right|^2 \left(x'\cos\theta + y'\sin\theta\right)^2 \, dx'dy'. \tag{3}$$

Equation 3 is the "second electrical moment" of the slice of target in the θ direction. Target shape information, in the form of scattering center moments weighted by local scatterer strength, can be deduced from a set of measured values of g by determining the parameter κ^2 that best fits the statistics of the data to the probability density of Equation 2. Moreover, it is easy to see that $\kappa\left(\theta\right) \equiv \sqrt{\kappa^2\left(\theta\right)}$ defines an ellipse whose shape and orientation depend upon the cross-range extent of the target. When combined with time-domain data acquired from a narrow pulse, Equation 3 will yield a family of down-range ellipses which will "enhance" ordinary down-range profiles by providing additional (although limited) cross-range target structure information.
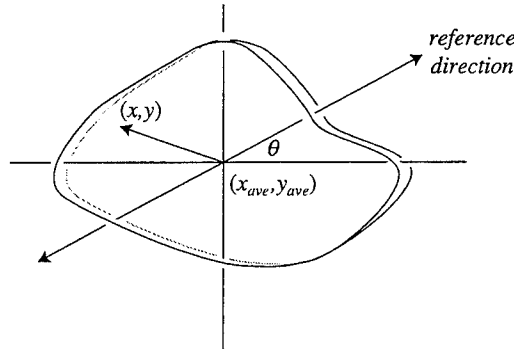

FIGURE 3. The Effective Target Slice.

The data used to estimate the "electrical moments of inertia" of an airborne target are the ordinary AOA measurements used by radar tracking systems. Since an airborne target will alter its orientation over time as it maneuvers (or even if it is flying "straight and level"), the AOA will fluctuate with time as well. (In the straight-flight case, the target orientation will typically vary randomly over several degrees in only a few seconds, resulting in significant variation in the AOA estimates.) The statistics of this variation are determined by the target orientation and the cross-range target structure in a known way. By fitting the statistics of the AOA measurements (collected over time) to this model, the relevant cross-range information can be determined for each slice.

The information obtainable is the overall target orientation and moment "ellipse" estimates for each range slice. (The moment ellipse has semi-axes defined by the electrical moments of inertia.) In
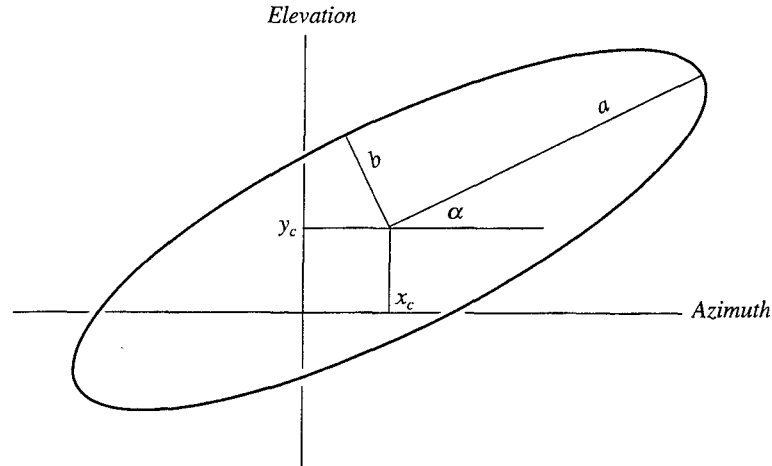
3

FIGURE 4. Ellipse Parameter Definition. These five parameters encode the cross-range target information available for each down-range slice.

particular, each range slice is mapped to an ellipse which is defined by the five parameters described by Figure 4. The collection of all range slice ellipses associated with a target at a particular aspect defines the total available target structure and orientation information.

MONOPULSE THERMAL NOISE ERROR

One of the potential problems with this idea is the dynamic range and signal-to-noise (S/N) power ratio available to AOA measurement systems. In general, when thermal noise is absent, a wideband radar that broadcasts a pulse—sufficiently narrow to illuminate only a single scattering center on the target at an instant (as in Figure 1)—will measure AOA data whose dynamic range is limited to the target's cross-range extent divided by the target's range. When there are two (or more) scatterers simultaneously illuminated by the radar pulse, however, scintillation effects will *increase* the dynamic range of the AOA measurements—typically, by a factor of 4 or more. All else being equal, the net effect is that the range at which the target's cross-range structure will affect the AOA measurements will be increased by the same factor.

Thermal noise effects manifest themselves by introducing a random Gaussian component to the AOA measurements (Reference 4). For a target on the antenna axis, and assuming a large S/N ratio, the noise voltage for a single pulse can be expressed in terms of the reference voltage as

$$E_n = \frac{E_r}{\sqrt{S/N}}. \tag{4}$$

If the detector has unit-gain error, then the rms noise voltage is just $E_{n(rms)} = E_n/\sqrt{2}$. This noise voltage will enter the system as an apparent (additive) signal voltage and so is related to the rms

angle error σ by the usual monopulse voltage-to-angle conversion factor Θ/k_m:

$$\sigma = \frac{\Theta}{k_m\sqrt{2S/N}}. \tag{5}$$

Here, Θ is the antenna beamwidth and k_m is the monopulse error slope (Reference 5). Note that if the measurements from n pulses are averaged together, then the rms error of Equation 5 will be reduced by a factor of $1/\sqrt{n}$.

This simple analysis allows for some "back-of-the-envelope" style observations about the use of AOA measurements in target cross-range estimation. To begin with, a "simple" target (i.e., with one non-scintillating scatterer per range bin) with cross-range dimension d cannot generate rms AOA data greater than $d/2$. In the presence of noise, the data will not be discerned in the measurements unless they are (approximately) greater than the rms noise error. If R denotes the radar-to-target range, then this implies that the data will have little value if

$$\sigma > \frac{d}{2R}. \tag{6}$$

Using Equations 5 and 6 we can estimate the range for which AOA measurements can be applied to cross-range estimation *of simple target* characteristics as

$$R < \frac{k_m d\sqrt{2S/N}}{2\Theta}. \tag{7}$$

A 10m target, for example, being observed by an X-band monopulse tracking system with $\Theta = 15°$, $k_m = 1.5$, and $S/N = 10^5$ would not display discernible cross-range information until $R < 12$km.

Another easy consequence of Equation 5 is the dependence of radiation frequency upon rms angle error. For fixed radar antenna size, the associated beamwidth varies in proportion with the wavelength—the proportionality factor depending on the antenna shape and feed configuration (Reference 6). This is related to the concept of "imaging resolution." For the present discussion, and to the current approximations, this has the effect of scaling the results by the appropriate wavelength-related amount: the range limit in the above example (based on Equation 7) will be increased to over 100 km if the radar frequency is changed from 10 to 94 GHz.

There are some problems with this notion of beamwidth reduction. In particular, narrow beams will be less likely to detect a target in the first place and will also allow rapidly maneuvering targets to more easily slip into an antenna sidelobe. In contrast to simple targets, however, it is a feature of scintillating targets with cross-range dimension d that the AOA data are *often* greater than $d/2$. This has the consequence of further diminishing the effects of thermal noise and extending the range limit of Equation 7.

DATA ERROR STATISTICS

To understand how scintillation can significantly increase the dynamic range of AOA measurements (over those from non-scintillating targets), consider the following analysis (Reference 7).

Fix a coordinate system to the target and examine a monostatic scattering situation in which the transmitter and receiver are co-located. The weak scatterer approximation far-field response

$E(\mathbf{k})$ due to a harmonic excitation of a target can be written as a linear superposition of waves with strength $|\rho(\mathbf{r})|$ radiating from location $\mathbf{r}$:

$$E(\mathbf{k}) = \int_D \rho(\mathbf{r}) \exp(i\mathbf{k} \cdot \mathbf{r}) \, d\mathbf{r}. \tag{8}$$

Here, D is the support of the local scatterer density function $\rho(\mathbf{r})$ (scaled by range), $\mathbf{k}$ is the wave vector with $|\mathbf{k}| = 2\pi f/c = 2\pi/\lambda$, c is the speed of wave propagation, f the wave frequency and λ the wavelength. (We have suppressed the $\exp(-i2\pi ft)$ time dependence.) This far-field approximation can be expected to be quite accurate up to the late end-game, at which point additional missile guidance corrections are usually treated as having only limited effectiveness. Moreover, since missile antennas are almost always mounted on moving gimbals so that the target can be "held" to lie within the near-linear region of the antenna pattern, it is relatively easy to correct the response (Equation 8) for variations in the receive aperture. (Consequently, this aperture variation presents only a minor complication and will not be considered in the following.)

Consider values of $\mathbf{k}$ restricted to lie within a plane containing both the target and the radar. If ζ denotes target aspect in this plane (see Figure 5), then Equation 8 can be written

$$E(f, \zeta) = \int_D \rho(x, y) \exp(i(2\pi f/c)(x \sin\zeta - y \cos\zeta)) \, dx \, dy, \tag{9}$$

where now $\rho(x, y)$ represents the source function integrated along the direction orthogonal to the x–y plane. Denote $\xi \equiv (2\pi f/c) \sin\zeta$ and $\psi \equiv -(2\pi f/c) \cos\zeta$. In the usual small-angle approximation, $\xi \approx 2\pi f\zeta/c$ and $\psi \approx -2\pi f/c$, and we can write Equation 9 as the iterated integral

$$E_f(\xi) = \int_a^b \tilde{\rho}_f(x) \exp(i\xi x) \, dx \tag{10}$$

where $\tilde{\rho}_f(x) \equiv \int \rho(x, y) \exp(-i2\pi fy/c) \, dy$ and each integral has limits appropriate to the target support. (In particular, $\tilde{\rho}_f(a), \tilde{\rho}_f(b) \neq 0$.)

Equation 10 can be used to continue $E_f(\xi)$ into the complex w–plane so that

$$E_f(w) = \int_a^b \tilde{\rho}_f(x) \exp(iwx) \, dx. \tag{11}$$

If the support interval (a, b) is finite, then $E_f(w)$ is an entire function of exponential type and can be represented by the Weierstrass canonical product. On the real–w axis we can write (Reference 8)

$$E_f(\xi) = E_f(0) \exp\left(i\frac{a+b}{2}\xi\right) \prod_{n=1}^{\infty}\left(1 - \frac{\xi}{w_n}\right). \tag{12}$$

This product represents the scattered field as a function of the *real* variable $\xi = 2\pi f\zeta/c$ in factors of the *complex* zeros of the field continued into the complex plane.

The quadrature phase $\phi_f(\xi)$ of the scattered field is defined by $E_f(\xi) = |E_f(\xi)| \exp(i\phi_f(\xi))$. The derivative of this phase can be found from Equation 12 as

$$g \equiv \frac{c}{2\pi f}\frac{\partial \phi_f(\xi)}{\partial \zeta} = \frac{a+b}{2} + \frac{\zeta}{2}\frac{\partial}{\partial \zeta}(a+b) + Im\left(\sum_{n=1}^{\infty}\frac{1}{2\pi f\zeta/c - w_n}\right). \tag{13}$$

FIGURE 5. Target Scattering Coordinates. The target and the radar both
lie in the plane of the paper.

This is the glint error in units of the linear cross-range coordinate at the target and can be expected
to be valid over a small range of aspect angles for which the locations of the zeros can be taken as
fixed.

Equation 13 is proportional to the pointing angle away from the origin of the coordinate system
fixed within the target and displays all the behavior associated with glint (for example, it displays
the strong correlation between glint spikes and amplitude fades (Reference 9)). When $(a + b)$ is a
slowly varying function of aspect, the second term will be vanishingly small. The first term does
not vary with small changes in aspect and $\frac{1}{2}(a + b)$ is known as the cross-range tracking "centroid"
of the target. As we have discussed, larger aspect variations will often be accompanied by changes
in the value of $(a + b)$ and so the centroid will vary in position. (This is known as "bright-spot
wander".) If the change in centroid position is rapid enough, then the second term in Equation 13
can take on large transient values and we may observe associated spike-like behavior. Note that
since this spike-like behavior is associated with a rapid change in $(a + b)$, it will generally separate
the domain of $\partial \phi_f(\zeta)/\partial \zeta$ into subdomains over which Equation 13 is valid to within the small angle
approximation: in each subdomain, a, b, and $\{w_n\}$ can be assumed to be approximately fixed.

Within each of these subdomains there is also a regular spike-like behavior determined by the
third term of Equation 13. The $\{w_n\}$ are defined as the points on the complex w–plane at which
$E_f(w)$ vanishes. If we write $w_n = Re\,(w_n) + i\,Im\,(w_n)$, then

$$Im\left(\sum_{n=1}^{\infty} \frac{1}{2\pi f\zeta/c - w_n}\right) = \sum_{n=1}^{\infty} \frac{Im\,(w_n)}{\left(2\pi f\zeta/c - Re\,(w_n)\right)^2 + Im\,(w_n)^2} \qquad (14)$$

and we can see that a zero w_n can make a significant contribution to the sum in Equation 13 only
if it is located near the real axis.

Let $w_1 = |w_1| \exp(i\gamma_1), w_2 = |w_2| \exp(i\gamma_2), \ldots$, be the zeros arranged in order of increasing modulus. When $\tilde{\rho}_f$ is defined as in Equation 10 with $a \neq b$, the asymptotic form of the zeros is given by (Reference 10)

$$w_n = \frac{n\pi}{b-a} + i\,\frac{1}{2(b-a)} \ln\left(\frac{\tilde{\rho}_f(a)}{\tilde{\rho}_f(b)}\right) + \epsilon_n, \qquad (15\ )$$

where $\epsilon_n \to 0$ as $n \to \infty$. (If $a = b$ then the third term of Equation 13 vanishes.) $E_f(w)$ is known as a "sine-type" function and has zeros that lie (approximately) on a regular lattice determined by the support of $\tilde{\rho}_f$. If we write $\tilde{\rho}_f(x) = |\tilde{\rho}_f(x)| \exp(i\eta_f(x))$, then Equation 15 becomes

$$w_n = \frac{n\pi + \frac{1}{2}(\eta_f(b) - \eta_f(a))}{b-a} + i\,\frac{1}{2(b-a)} \ln\left|\frac{\tilde{\rho}_f(a)}{\tilde{\rho}_f(b)}\right| + \epsilon_n. \qquad (16\ )$$

Equations 13 and 16 allow us to make a qualitative description of glint. Denote the cross-range target size $(b-a)$ by d and the ratio $|\tilde{\rho}_f(a)/\tilde{\rho}_f(b)|$ by r. When $2\pi f\zeta/c = Re(w_n)$, $n = 1, \ldots, \infty$, the third term of Equation 13 adds an additional angular glint error of approximately

$$g_{\text{spike}} \approx \frac{2d}{\ln(r)}. \qquad (17\ )$$

(This approximation assumes the spike is large.) In practice, of course, there will be a finite number of such glint spikes within each subdomain of "fixed" a and b. However, the density of these zeros increases with increasing frequency. Note that the size of the error spike is determined by the behavior of $\tilde{\rho}_f$ near the end point of the interval (a, b), and that when $r \approx 1$, these spikes can become quite large—so large, in fact, that g_{rms} becomes infinite as $r \to 1$ (Reference 7).

Of course, Equation 17 represents the maximum extent of the angle excursions. To better understand the statistical behavior of the noisy measurements, we must combine the results of sections 1 and 2.

TARGET PARAMETER ESTIMATE ERROR

The statistical density function associated with a set of measurements, z_i where $z = g + n$ is known to be the sum of two terms (AOA data g and noise n), can, in principle, be determined from the known statistics of g and n:

$$f_z(z = g + n) = \int_{-\infty}^{\infty} f_g(g) f_n(z - g) dg, \qquad (18\ )$$

where f_z, f_g, and f_n are the probability density functions of the measured data, the noise-free AOA, and the measurement noise component, respectively.

For f_g given by Equation 2 the integral in Equation 18 is unwieldy for all but the simplest forms of f_n. Moreover, the determination of this integral (in closed-form) is inappropriate for our purposes, since we are concerned with the effects of the errors associated with "small" data sets and not the asymptotic behavior usually studied in the standard texts. Consequently, we will adopt the simple expedient of computer modeling: a random "noise" term will be added to synthetically generated AOA "data" and processed by a maximum likelihood algorithm to estimate κ^2. The estimate will be compared to the "noise-free" value and the process repeated to establish an "error statistic".

8

Assuming the model of Equation 2 is accurate, then the maximum likelihood estimator for κ^2 will be the one that maximizes the function

$$\Lambda\left(\kappa^2\right) = \prod_{i=1}^{N} \frac{\kappa^2/2}{\left(\kappa^2 + z_i^2\right)^{3/2}} \tag{19}$$

over a set of data $\{z_i\}_{i=1,\dots,N}$. When $n_i = 0$ ($\sigma = 0$), then $z_i = g_i$ and the maximum likelihood estimate will be asymptotically convergent to the correct model parameter κ^2 (i.e., when $N \to \infty$). Of course, the point of this discussion is that, in practical situations, $\sigma \neq 0$ and $N \ll \infty$.

Differentiating $\ln \Lambda\left(\kappa^2\right)$ with respect to κ^2 and setting the result to zero yields

$$\frac{N}{3} - \sum_{i=1}^{N} \frac{\kappa^2/2}{\kappa^2 + z_i^2} = 0. \tag{20}$$

Equation 20 is the sum of functions of the form

$$\frac{1}{3} - \frac{\kappa^2/2}{\kappa^2 + z_i^2} \tag{21}$$

and so it will possess only two real solutions which are located symmetrically about the origin. The magnitude of either zero is our desired estimate and can be obtained numerically from Equation 20.

Define a simple target model as in Figure 6. The target is composed of M point scatterers lying along a line segment of length d rotated by an angle ζ ($\zeta \sim 0$) with respect to the radar axis. The amplitude $A_j = A$ for each point scatterer while the phase shift ϕ_j is chosen to be uniformly random within $\{-\pi, \pi\}$. The position of each point scatterer is also uniform in $\{-d/2, d/2\}$.

For our simulation we set the model using a random number generator and determine the far-field AOA that would be measured by an ideal radar system for a selected value of ζ:

$$g = \frac{c}{2\pi f} \frac{\partial \phi(\zeta)}{\partial \zeta} = \frac{ru + sv}{r^2 + s^2}, \tag{22}$$

where $r \equiv \sum_{j=1}^{M} \cos p_j$, $s \equiv \sum_{j=1}^{M} \sin p_j$, $u \equiv \sum_{j=1}^{M} x_j \cos p_j$, $v \equiv \sum_{j=1}^{M} x_j \sin p_j$, and $p_j \equiv \phi_j + x_j 2\pi f \zeta / c$. Random noise is generated and added to form a data point $z = g + n$ associated with each ζ.

The data set to be processed (by solving Equation 20) is formed by creating N such simulated AOA values $z_i = z(\zeta_i)$ for N corresponding values of ζ (chosen as uniformly and randomly distributed within $\{-1°, 1°\}$). By repeating this process over many data sets, we can get a feel for how the estimation process behaves for particular values of the parameters σ and N. Finally, by further varying σ and N, we can estimate the performance of the algorithm under limited and noisy data constraints.

Denote the fractional difference between the value of κ estimated from the data (using Equation 20) and its true value by Δ. For the model of Figure 6 we have

$$\kappa_{true} = \sqrt{\frac{1}{M} \sum_{j=1}^{M} (x_j - x_{ave})^2}, \tag{23}$$
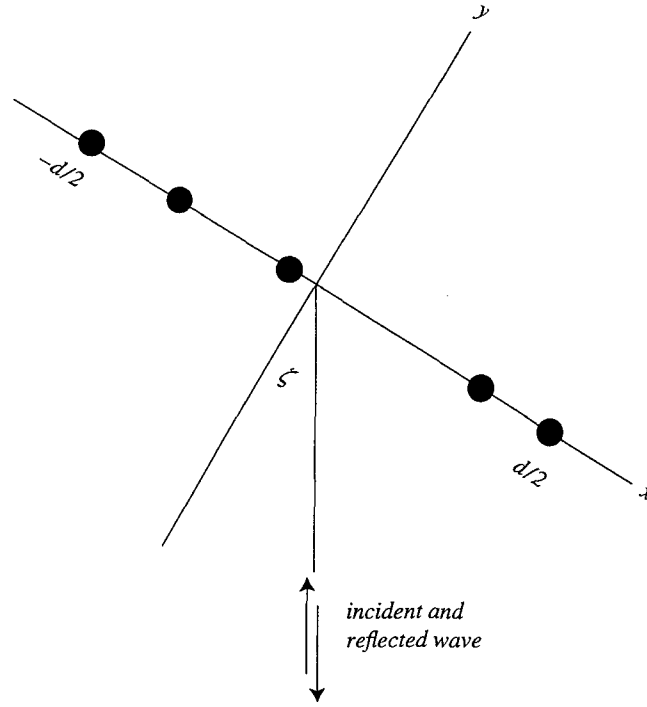
FIGURE 6. Simple M-Point Target Scattering Model.

where x_{ave} denotes the average value of $\{x_j\}$. Then

$$\Delta = \frac{\kappa_{est} - \kappa_{true}}{\kappa_{true}}. \tag{24}$$

Equation 22 expresses the "AOA" error in units of length measured at the location of the target. For ease of interpretation, the noise error's standard deviation σ will be expressed as a fraction of $d/2$—the conversion to more common (angular) units being straightforward (divide by range). Figure 7 is the error Δ associated with an $M = 10$ scatterer target and plotted as a function of the varying parameters σ and N. Each value $\Delta(\sigma, N)$ was obtained by averaging the results of 2000 model simulations.

The results displayed in Figure 7 clearly show the deleterious effects of additive noise. The noise-free results (representative of the data used in our previous reconstructions (References 1 and 2)) are represented by the $\sigma = 0$ curve and indicate that the relative error is less than about 10%, if the data set consists of more than about 20 points. This trend is maintained over the study and even when $\sigma = .21(d/2)$, the relative error is less than about 15% for data sets consisting of more than 30 points. For larger values of σ or smaller data sets, the results get progressively worse. We have found that our ellipse estimation algorithm yields "inconclusive" results when $\Delta > .25$, although this is difficult to quantify.

Figure 8 is a similar plot of the effects of measurement error, but for a target composed of twice as many ($M = 20$) scatterers as in Figure 7. Note that the pattern of effects of noise and data number are nearly identical to those displayed in Figure 7.
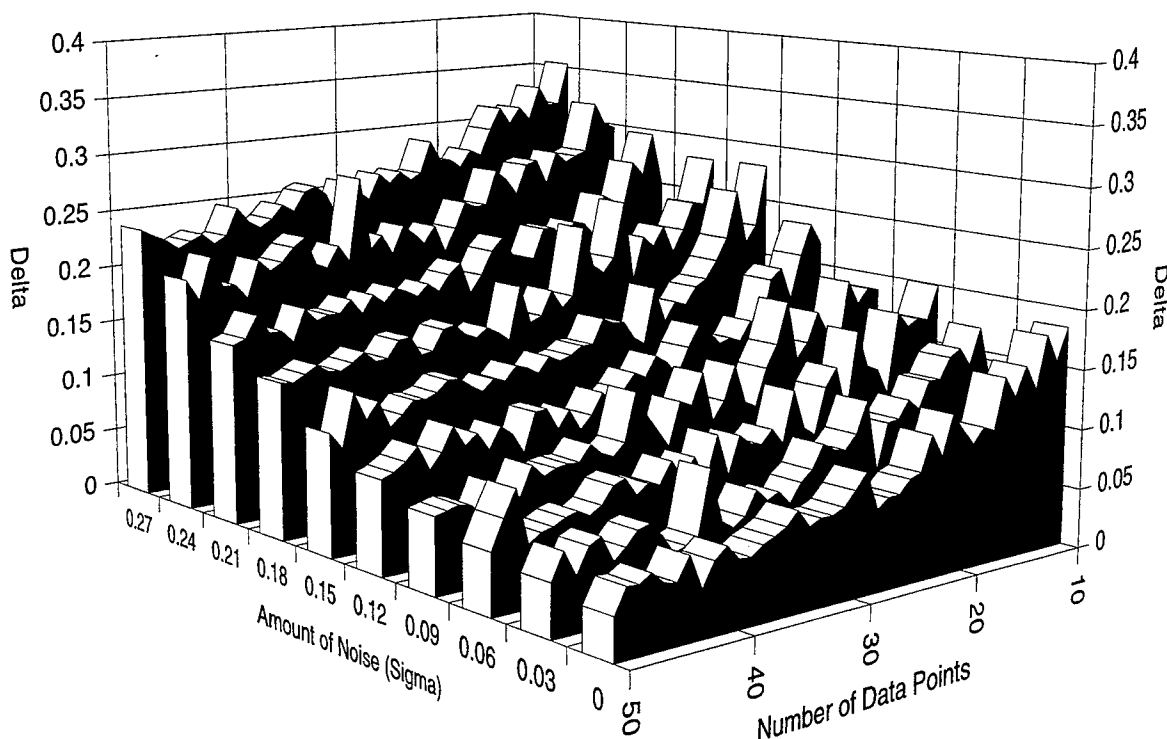
FIGURE 7. Estimation Error Dependence Upon Magnitude of Noise and Number of AOA Measurements. The target was as in Figure 6 with M=10, d=10m, f=35GHz. The parameter σ is expressed in units of $d/2$.

CONCLUSION

The foregoing analysis has reviewed a statistical technique for extracting target cross-range information from radar AoA (tracking) data. When this information is collected by a radar system that is also wideband, then the ordinary range-profiles used for target classification/identification can be "enhance" to yield significantly more relevant information than would otherwise be available to the observer (Reference 2).

The data collection technique is subject to random noise contamination which has the effect of altering the statistics presumed in the development of the enhanced range-profile algorithm. It is natural to ask if the statistics are sufficiently altered so that the algorithm will fail to perform in an acceptable fashion. Moreover, since the algorithm was originally developed using suppositions appropriate to asymptotically large data sets and asymptotically dense collections of target sub-scatterers, it is also natural to ask if the algorithm fails when these model assumptions are relaxed.

We have performed a "brute-force" analysis of the effects of including random measurement error and reducing the size of the collected data set. Basically, we simply sampled 2000 pseudo-random generated elements of an "ensemble" associated with a simple (linear) target for a given number of data points and a given amount of additive noise, and applied our algorithm to each element. By comparing the estimated results with the actual moments associated with the target, we were able to obtain an approximate "reliability" figure for the algorithm under varying conditions
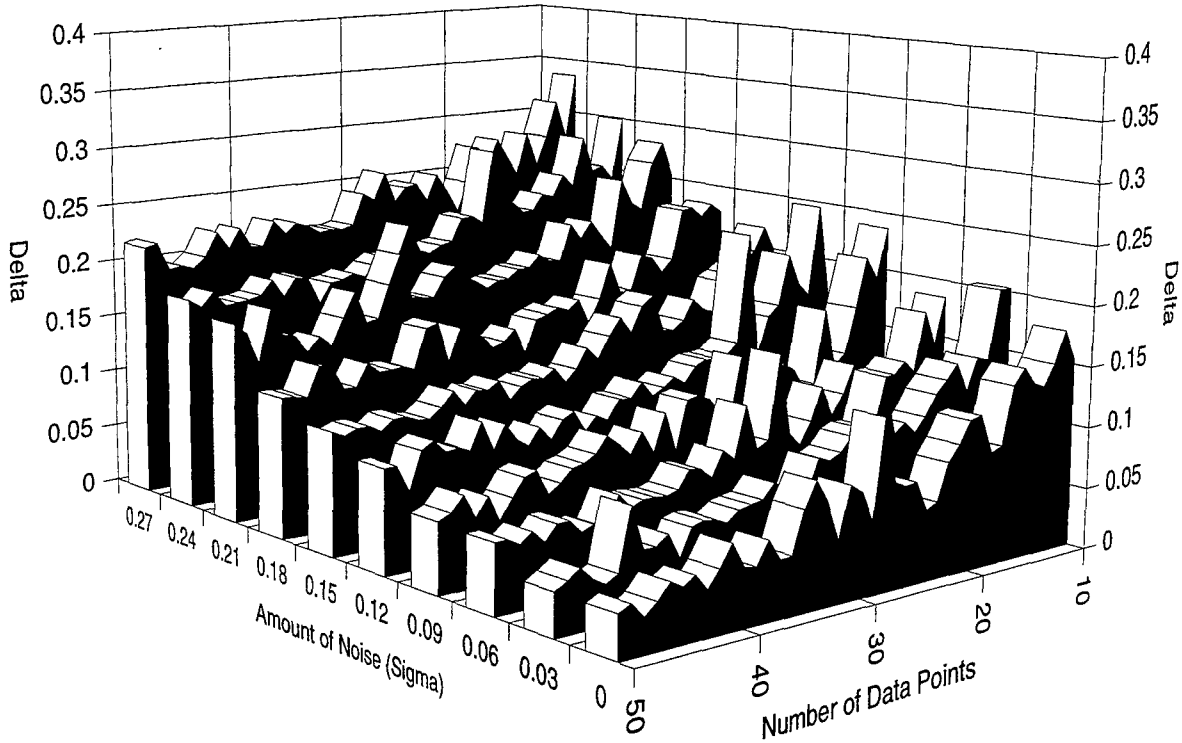
FIGURE 8. Estimation Error Dependence Upon Magnitude of Noise and Number of AOA Measurements. The target was as in Figure 6 with M=20, d=10m, f=35GHz. The parameter σ is expressed in units of $d/2$.

(see Figures 7 and 8).

As a result, we believe the algorithm displays gradual (noncatastrophic) failure as the noise level is increased or the number of measured data values is reduced. Moreover, our results indicate that the algorithm can be expected to yield useful results when the number of data points is larger than ~ 30 and the additive (angular) noise is less than $\sigma \sim .25(d/2)$ (measured in units of length at the location of the target). Consequently, this analysis allows us to refine the analysis leading up to Equation 7 and we can say that AOA measurements can be applied to cross-range estimation when

$$R < .25\ \frac{k_m d\sqrt{2S/N}}{2\Theta}. \tag{25}$$

This reduces the discrimination range of our previous example (text following Equation 7) from $R < 12$km to $R < 3$km. This is a problematic range and is an effective argument for higher radar frequencies and associated narrower beamwidths.

REFERENCES

1. B. Borden. "Problems in Radar Target Recognition," *Inverse Problems,* Vol. 10 (1994), pp. 1009-22.

2. B. Borden. "Enhanced Range Profiles for Radar-Based Target Classification Using Monopulse Tracking Statistics," *IEEE Trans. Antennas and Propag.,* Vol. 43 No. 8 (1995), pp. 759-65.

3. D. D. Howard. "High Range-Resolution Monopulse Tracking Radar," *IEEE Trans. Aerospace and Electr. Sys.,* Vol. 11 No. 5 (1975), pp. 749–55.

4. D. K. Barton. *Radar Systems Analysis,* Dedham, Mass., Artech House, Inc., 1976.

5. S. M. Sherman. *Monopulse Principles and Techniques.* Dedham, Mass., Artech House, Inc., 1984.

6. S. Silver. *Microwave Antenna Theory and Design.* New York, McGraw-Hill, 1949.

7. B. Borden. "Requirements for Optimal Glint Reduction by Diversity Methods," *IEEE Trans. Aerospace and Electr. Sys.,* Vol. 30 No. 4 (1994), pp. 1108–14.

8. E. C. Titchmarsh. "The Zeros of Certain Integral Functions," *Proc. London Math. Soc.,* Vol. 25 (1925), pp. 283–302.

9. C. M. Nullin and B. Aas. "Experimental Investigation of Correlation Between Fading and Glint for Aircraft Targets," *Radar-87 Conference Proceedings,* October 1987. Pp. 540–43.

10. M. L. Cartwright. "The Zeros of Certain Integral Functions," *Quarterly J. Math.,* Oxford Ser. 1, Vol. 1 (1930), pp. 38–59.

INITIAL DISTRIBUTION

4 Naval Air Systems Command, Arlington
    AIR-4.1.1 (1)
    AIR-4.1.8
      File (1)
      Stegman (1)
    AIR-4.10A (1)
2 Defense Technical Information Center, Alexandria
2 Center for Naval Analyses, Alexandria, VA
    Dr. A. Borden (1)
    L. Lynn (1)

ON-SITE DISTRIBUTION

1 Code 455560D, W. Katzenstein
1 Code 455580D, D. Reade
2 Code 4713C0D
    G. Hewer (1)
    R. Smith (1)
1 Code 472230D, D. Paolino
1 Code 4726G70D, G. Winkler
1 Code 473A20D, M. Mumford
2 Code 474400D
    B. Borden (1)
    S. Chesnut (1)
4 Code 474710D (3 plus Archives copy)
1 Code 474T60D, T. Loftus